Title

Oligodendrocytes that survive acute coronavirus infection induce prolonged inflammatory responses in the CNS.

Journal

Proceedings of the National Academy of Sciences, 117(27)

Authors

Pan, Ruangang

Zhang, Qinran

Anthony, Scott

et al.

Publication Date

2020-07-07

DOI

10.1073/pnas.2003432117

Peer reviewed

Oligodendrocytes that survive acute coronavirus infection induce prolonged inflammatory responses in the CNS

Ruangang Pan[a], Qinran Zhang[b], Scott M. Anthony[a], Yu Zhou[b], Xiufen Zou[b], Martin Cassell[c], and Stanley Perlman[a,1]

[a]Department of Microbiology and Immunology, University of Iowa, Iowa City, IA 52242; [b]School of Mathematics and Statistics, Wuhan University, 430072 Wuhan, China; and [c]Department of Anatomy and Cell Biology, University of Iowa, Iowa City, IA 52242

Edited by Michael B. A. Oldstone, Scripps Research Institute, La Jolla, CA, and approved May 21, 2020 (received for review February 25, 2020)

Neurotropic strains of mouse hepatitis virus (MHV), a coronavirus, cause acute and chronic demyelinating encephalomyelitis with similarities to the human disease multiple sclerosis. Here, using a lineage-tracking system, we show that some cells, primarily oligodendrocytes (OLs) and oligodendrocyte precursor cells (OPCs), survive the acute MHV infection, are associated with regions of demyelination, and persist in the central nervous system (CNS) for at least 150 d. These surviving OLs express major histocompatibility complex (MHC) class I and other genes associated with an inflammatory response. Notably, the extent of inflammatory cell infiltration was variable, dependent on anatomic location within the CNS, and without obvious correlation with numbers of surviving cells. We detected more demyelination in regions with larger numbers of T cells and microglia/macrophages compared to those with fewer infiltrating cells. Conversely, in regions with less inflammation, these previously infected OLs more rapidly extended processes, consistent with normal myelinating function. Together, these results show that OLs are inducers as well as targets of the host immune response and demonstrate how a CNS infection, even after resolution, can induce prolonged inflammatory changes with CNS region-dependent impairment in remyelination.

coronavirus | virus-induced demyelination | oligodendrocyte | neuroinflammation

The etiology and pathogenesis of multiple sclerosis (MS), a human demyelinating disease, remain poorly defined, although autoreactive T cells and possibly environmental factors, especially viruses, play important roles in disease onset and exacerbation (1, 2). Viral infection has been implicated in the initiation and exacerbation of disease, although no single virus has been established as the etiological agent for any part of these processes, making any conclusions tentative. One possible explanation for this inability to identify one or more viral pathogens as the causative agent for subsequent demyelination is that the virus may be cleared by the time that brains and spinal cords are analyzed. The central nervous system (CNS) of MS patients is most often examined post mortem at autopsy, which is expected to occur months to years after a putative initiating viral brain infection.

Myelin-producing oligodendrocytes (Ols) are the primary targets for the autoimmune response in MS (1). Recent studies have extended our understanding of OL function and also demonstrated extensive heterogeneity of these cells (3). OL gene expression changes dynamically during development and also during normal myelin turnover that occurs either physiologically or after myelin destruction (4, 5). Furthermore, recent results also demonstrated expression of immune-associated genes, including those associated with major histocompatibility complex (MHC) class I and class II expression, by OLs and oligodendrocyte precursor cells (OPCs) at the peak of experimental autoimmune encephalomyelitis (EAE) (6, 7). Whether viral antigen persists in oligodendrocytes or other cells in the CNS for extended periods of time after resolution of infection is unknown, but if it occurs, it might enhance the inflammatory process and possibly contribute to ongoing demyelination.

Mouse hepatitis virus strain rJ2.2 (MHV) is an attenuated neurotropic betacoronavirus that causes mild acute encephalitis and acute and chronic demyelinating disease (8). MHV is related to severe acute respiratory syndrome coronavirus (SARS-CoV), Middle East respiratory syndrome coronavirus, and SARS-CoV-2, the newly identified cause of pandemic pneumonia in China and elsewhere (9, 10). MHV shares ∼52.5% nucleotide identity with SARS-CoV-2. The vast majority of mice (∼90%) survive the acute infection but then develop a demyelinating disease that mostly resolves by 25 to 45 d. During the chronic phase of disease, the most commonly infected cells are OLs although microglia/macrophages and astrocytes are also infected to a limited extent (8). Demyelination occurs during the process of virus clearance, followed by remyelination as the inflammatory process resolves. Most mice develop demyelination, but the extent of myelin destruction is variable among mice. Infectious MHV is cleared by 10 to 14 d post infection (dpi), but viral RNA can be detected several months after infection (11, 12). Virus antigen is usually undetectable by immunohistochemistry by 14 dpi although it can occasionally be detected at 2 mo post infection (p.i.) (13). Adoptive

Significance

Both genetic and environmental factors, especially viruses, may contribute to the development of multiple sclerosis. In this study, we find that oligodendrocytes (OLs) survive infection with a neurotropic coronavirus, the mouse hepatitis virus, for at least 150 d. These surviving OLs are located adjacent to demyelinating regions and express genes that contribute to a chronic inflammatory state. Notably, the extent of inflammatory cell infiltration and subsequent ability to regain normal OL morphology varied depending upon anatomic location in the central nervous system (CNS). Together, these results reveal an unexpected capacity for infected cells to survive in the CNS and also indicate that the inflammatory response and apparent ability to contribute to remyelination differs in different regions of the CNS.

Author contributions: R.P. and S.P. designed research; R.P. performed research; Q.Z., S.M.A., Y.Z., and X.Z. contributed new reagents/analytic tools; R.P., Q.Z., Y.Z., X.Z., M.C., and S.P. analyzed data; and R.P. and S.P. wrote the paper.

The authors declare no competing interest.

This article is a PNAS Direct Submission.

Data deposition: Next-generation RNA sequence data supporting the findings in this study have been deposited in the Gene Expression Omnibus database (https://www.ncbi.nlm.nih.gov/geo/) under accession number GSE148650.

[1]To whom correspondence may be addressed. Email: stanley-perlman@uiowa.edu.

This article contains supporting information online at https://www.pnas.org/lookup/suppl/doi:10.1073/pnas.2003432117/-/DCSupplemental.

First published June 22, 2020.

transfer of bone marrow from uninfected congenically mismatched mice to infected mice at 33 dpi results in the outgrowth of MHV-specific T cells from the donor bone marrow, suggestive of some degree of MHV antigen presentation (13). However, from these results, it is not possible to assess the relationship between prior infection and demyelination at the cellular level. In particular, cells that were infected and survived long-term might play important roles in ongoing demyelination, but whether this occurs and to what extent is unknown.

To understand the role of prior MHV infection in ongoing demyelination, we followed a previously described strategy for lineage tracing (14, 15). We engineered a recombinant MHV that expressed Cre recombinase and infected mice that expressed a "floxed" tdTomato (B6;129S6-*Gt[ROSA]26Sor*$^{tm14(CAG-tdTomato)Hze}$/J, Ai14) under a ubiquitous promoter (Rosa26). This in vivo tracing system allowed us to detect surviving, previously infected cells in the CNS for at least 150 d. The results showed that these cells were associated with areas of demyelination, with greater myelin destruction observed in areas with increased numbers of microglia/macrophages and CD8 T cells. They also suggested that previously infected cells present in areas with less inflammatory changes were more likely to regain morphological changes consistent with a myelinating phenotype.

Results

Engineering Recombinant MHV Expressing Venus or Cre. To assess the role of cells that became infected and ultimately survived in mice with demyelinating lesions, we constructed two variants of recombinant MHV (rMHV). In both cases, a foreign protein was inserted into ORF4, a site that is required for neither virus replication nor virulence (Fig. 1*A*) (16). After insertion of Venus, infection with the resulting virus (rMHV$_{Venus}$) allowed detection of acutely infected cells. A second recombinant virus encoded Cre, and after infection of Ai14 mice, surviving cells permanently expressed tdTomato (rMHV$_{Cre}$) (Fig. 1*B*). Cre expression was stable for at least seven passages in a fibroblast cell line (Fig. 1*C*). Venus expression was detected as early as 12 h after infection (Fig. 1*D*). Furthermore, infection with rMHV$_{Venus}$, rMHV$_{Cre}$, or rMHV resulted in similarly sized plaques in tissue culture cells (Fig. 1*D*). All viruses caused the same amount of weight loss with maximal effects at 7 to 10 dpi and replicated to a similar extent in the CNS when titers were measured at day 5 p.i., the peak of infection (Fig. 1*E*). Infection with rMHV$_{Cre}$ resulted in tdTomato expression at well-defined sites in the brain (Fig. 1*F* and see below).

Surviving, Previously Infected Cells in the CNS Are Predominantly Oligodendrocytes. We next determined whether cells that had been infected survived the acute infection and could be detected for extended periods of time and whether their numbers were stable. For this purpose, we infected Ai14 mice with rMHV$_{Venus}$ or rMHV$_{Cre}$ and monitored Venus and tdTomato expression. Venus expression was maximal at 10 to 14 dpi, lagging modestly behind times of peak virus replication (5 to 7 dpi) (8, 17), decreased by day 20 p.i., and was generally undetectable by 30 to 40 dpi (Fig. 2*A*). In contrast, 0.1 to 0.6% of cells in the rMHV$_{Cre}$-infected Ai14 CNS expressed tdTomato, and these cells could be detected for at least 150 d.

The majority of rMHV$_{Venus}$-infected cells were microglia and macrophages (CD11b^{+}CD45^{+}) at 10 dpi, but by 20 to 30 dpi, most were nonmyeloid (CD45^{-}CD11b^{-}) cells (Fig. 2*B*). By contrast, the proportion of myeloid cells that were previously infected with rMHV$_{Cre}$ and survived the acute phase (tdTomato^{+}) decreased only 1.5- to 2-fold from 10 to 40 dpi, with concomitant increases in

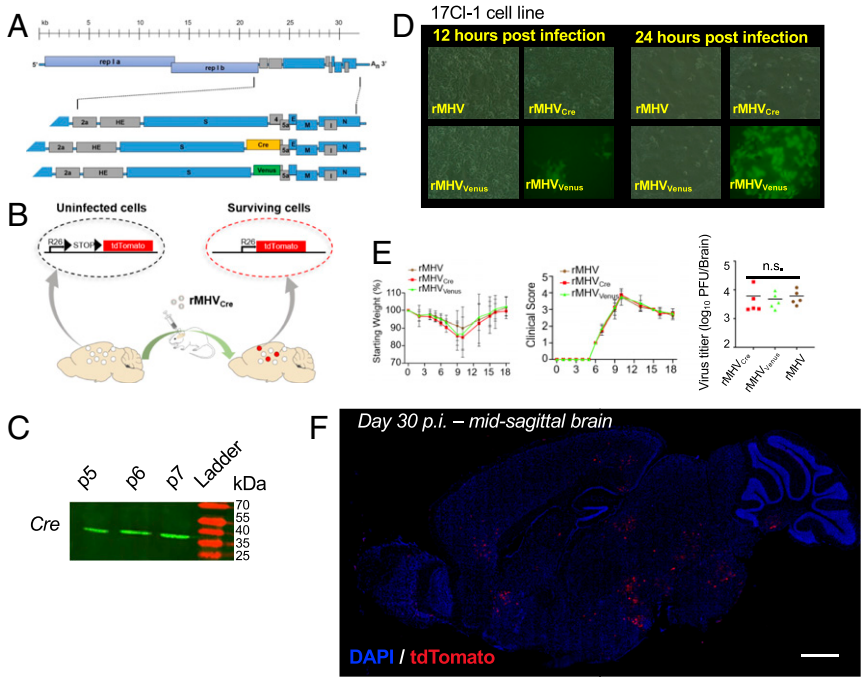

Fig. 1. Development and characterization of Cre- and Venus-expressing MHV. (*A*) Genome of recombinant MHV expressing either enterobacteria phage P1 Cre recombinase (rMHV$_{Cre}$, shown in yellow) or Venus (rMHV$_{Venus}$, shown in green). (*B*) Schematic shows that expression of Cre resulted in excision of loxP-flanked stop sites leading to tdTomato protein expression in rMHV$_{Cre}$-infected cells. (*C*) Cre expression was confirmed by Western blot analysis using antibodies specific for Cre. (*D*) Venus expression was confirmed by fluorescent microscopy using 17Cl-1 cells infected with rMHV$_{Venus}$ or mock infected. (*E*). Weights (*Left*) and clinical scores (*Middle*) of infected mice were monitored. rMHV, rMHV$_{Cre}$, or rMHV$_{Venus}$,-infected Ai14 mice develop indistinguishable clinical disease. (*Right*) Virus titers at day 5, the peak of infection. n.s., not significant. (*F*) Representative images of frozen midsagittal brain sections are shown at 30 d after intracranial injection of Rosa-tdTomato mice with 750 plaque-forming units (PFUs) of rMHV$_{Cre}$. tdTomato+ cells are red and DAPI-stained nuclei are blue. See also *SI Appendix*, Fig. S2. Data are representative of three independent experiments.

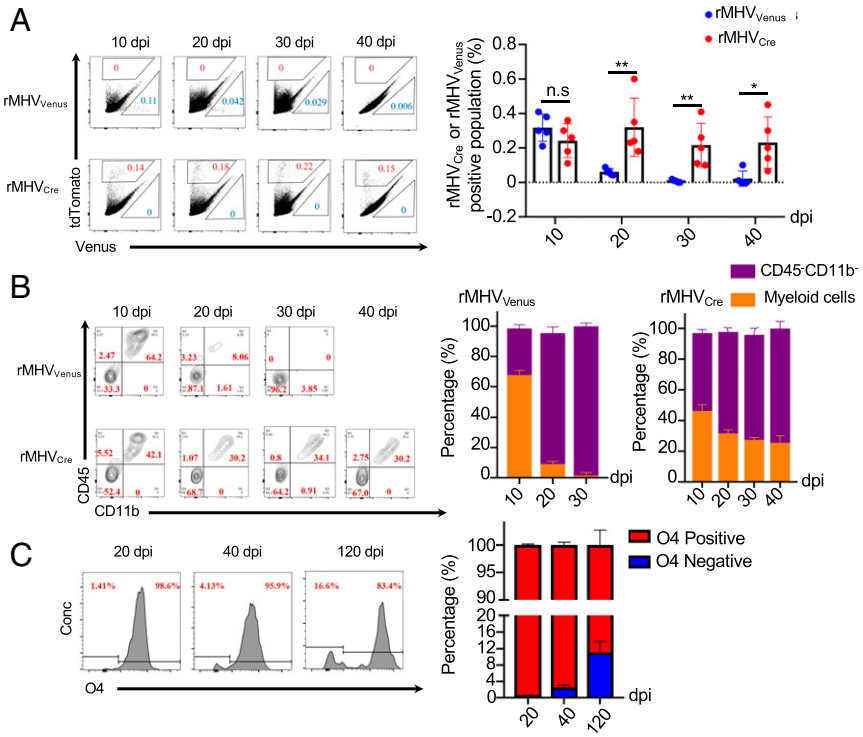

Fig. 2. Time course of tdTomato and Venus expression in infected mice. Mice were infected intracranially with the indicated virus (750 PFUs/mouse). Infected mice were killed at the indicated times, and combined brains were harvested and analyzed by flow cytometry. (*A*) tdTomato$^+$ and Venus$^+$ populations in the brain are shown. Venus$^+$ cells (blue, n = 5 mice/time point) were cleared more quickly than tdTomato$^+$ cells (red, n = 5 mice/time point). (*B*) Venus$^+$ and tdTomato$^+$ populations were analyzed for CD11b and CD45 expression. Few Venus$^+$ cells were detected by 20 dpi, and all were CD11b$^-$/CD45$^-$. Frequency of tdTomato$^+$ cells did not vary significantly up to 40 dpi although the fraction of CD11b$^-$/CD45$^-$ increased with time. (*C*) CD11b$^-$/CD45$^-$ tdTomato$^+$ cells in rMHV$_{Cre}$-infected mice were analyzed for O4 expression at the indicated time points (n = 8 mice/time point). *$P \leq 0.05$, **$P \leq 0.01$; two-tailed, unpaired Student's t tests were used in all panels.

the percentage of surviving nonmyeloid cells (Fig. 2*B*). By 90 dpi, we could detect tdTomato$^+$ microglia but not macrophages in the myeloid cell populations (*SI Appendix*, Fig. S1*A*). Although surviving CD45$^-$CD11b$^-$ cells in the CNS may include neurons, astrocytes, endothelial cells, and oligodendrocytes, the vast majority were OLs, as most of the nonmyeloid cells stained with O4 antibody, a marker of promyelinating and mature oligodendrocytes (Fig. 2*C*). These tdTomato$^+$ OLs underwent proliferation as measured by Ki67 expression, although to a variable extent compared to cells from mock-infected mice (*SI Appendix*, Fig. S1*B*). We also detected CD45$^-$CD11b$^-$ cells that were O4$^-$ at variable frequencies throughout the infection. While these cells have not been further characterized by flow cytometry, at least some of these cells were astrocytes, as assessed by confocal microscopy (see below).

Localization of tdTomato$^+$ Surviving Cells in the Brain. These results indicated that OLs were the predominant cells that had been infected with MHV and survived the acute infection. To confirm and extend these results, we next localized surviving cells within the brain by confocal microscopy (Fig. 1*F* and *SI Appendix*, Fig. S2). MHV preferentially infects cells in the olfactory and limbic systems, spreading from the olfactory bulb transneuronally to secondary and tertiary connections of the bulb (18, 19). In agreement with these results, cells that survived the acute infection were localized at 30 dpi primarily to sites associated with the olfactory system, including the olfactory bulb, piriform cortex, and fornix (*SI Appendix*, Fig. S2), and others, which are not primarily connected to the olfactory system, such as the subventricular zone (SVZ).

The specific type of surviving cell varied dependent upon anatomic location (Fig. 3 and *SI Appendix*, Fig. S3). Thus, surviving cells in the olfactory bulb were largely microglia/macrophages (Fig. 3 *A*, a_1), while those in the splenium were mature oligodendrocytes (Olig2$^+$CSPG4$^-$) and, to a lesser extent, astrocytes (GFAP$^+$), but not microglia/macrophages (Fig. 3 *B*, b_1; *C*, c_1, c_2; and *E*). OPCs were found in the splenium, but, using markers for OPCs (Olig2, CSPG4), we could not detect any tdTomato$^+$ OPCs at this site (Fig. 3*D*). However, tdTomato$^+$ OPCs were detected in the SVZ (Fig. 3 *F* and *H*, h_1), which is a primary site of OPC production. Most infected cells at some sites in the SVZ were Olig2$^+$ CSPG4$^+$ OPCs, while in adjacent areas, most were Olig2$^+$ CSPG4$^-$ OLs (Fig. 3 *F* and *H*, h_1). These data are summarized in Fig. 3*G*. Furthermore, tdTomato$^+$ OPCs persisted in the SVZ until at least day 60 p.i. (Fig. 3 *I*, i_1); whether prior infection inhibited differentiation of these cells requires further investigation.

tdTomato$^+$ Surviving Cells in the Spinal Cord Are Almost Exclusively Oligodendrocytes. The major site of MHV-induced demyelination is the spinal cord (20, 21). To assess whether specific types of cells preferentially survived the acute infection in the spinal cord, we used the cell-specific markers described above. First, we found, using flow cytometry, that most of the tdTomato$^+$ cells that survived infection in the spinal cord were in the white matter and were O4$^+$ OLs at day 30 p.i. (Fig. 4*A*). Second, we confirmed these results using confocal microscopy, where most tdTomato$^+$ cells were OLs as assessed by Olig2+ staining (Fig. 4*B*). Remyelination begins by day 14 p.i. (8), and as expected for lesions that are undergoing remyelination, OPCs were detected in

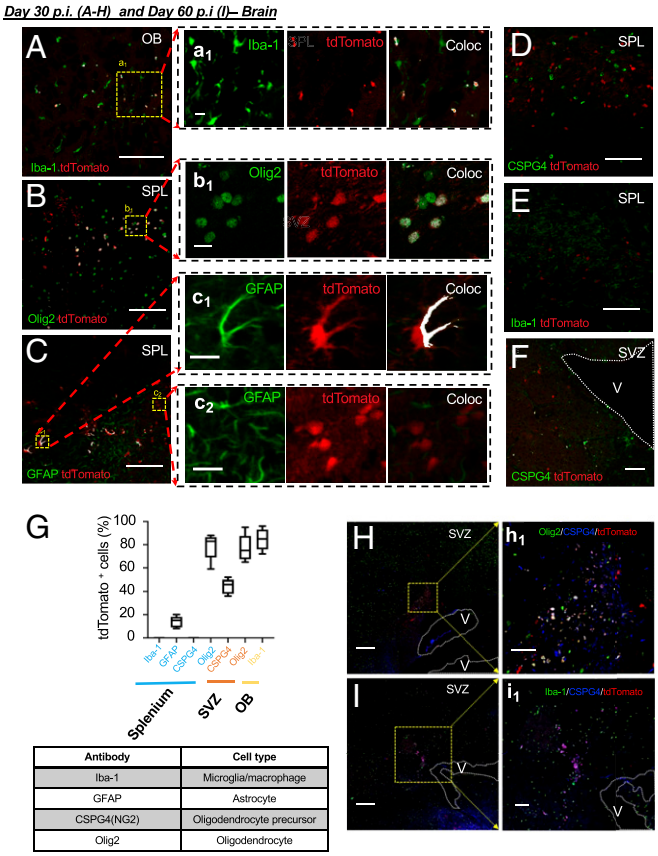

Antibody	Cell type
Iba-1	Microglia/macrophage
GFAP	Astrocyte
CSPG4(NG2)	Oligodendrocyte precursor
Olig2	Oligodendrocyte

Fig. 3. Regional differences in types of surviving cells in the brain. Confocal micrographs showing colocalization of tdTomato with Iba-1 (*A* and *E*), Olig2 (*B*), GFAP (*C*), and CSPG4 (*D* and *F*) in the olfactory bulb (OB, *A*), splenium (SPL, *B*–*E*), and SVZ (*F*) at 30 dpi. Boxed areas in *A*, *B*, and *C* are shown in a_1, b_1, c_1, and c_2, respectively. c_2 shows GFAP$^-$tdTomato$^+$ cells in the splenium, which are likely OLs (b_1). Images with colocalized cells are highlighted in white. Colocalization data were generated using ImageJ (*A*, *F*, and a_1–c_2). OLs and astrocytes but not OPCs colocalized with tdTomato in the splenium, while CSPG4$^+$ cells (OPCs) in the SVZ were tdTomato$^+$. Microglia/macrophages were the predominant tdTomato$^+$ cells in the OB. (*G*) Summary of the day 30 p.i. data (n = 9 mice) from three individual experiments (*Top*) and list of antibodies used for detection of each cell type (*Bottom*). (*H* and h_1) Olig2$^+$CSPG4$^+$ OPCs were detected in the SVZ at day 30 p.i.; Olig2$^+$CSPG4$^+$tdTomato$^+$ cells are pink and white. (*I*, i_1) CSPG4$^+$ cells (OPCs) were detected in the SVZ at day 60 p.i. Boxed areas in *H* and *I* are shown in h_1 and i_1, respectively. Ventricles (V) are indicated in *F*, *H*, *I*, and i_1. (Scale bars: *A*–*F*, 100 μm; a_1–c_2, 10 μm; *H* and *I*, 200 μm; h_1 and i_1, 50 μm.)

these white matter lesions (WML) at day 30 p.i. (Fig. 4*C*). The majority of these OPCs were not previously infected with virus, although some OPCs were tdTomato$^+$ (Fig. 4 *C* and *D*). Of the cells that were not oligodendrocytes, some in the gray matter were morphologically neurons, were localized near demyelinating lesions, and were GFAP$^-$Olig2$^-$CSPG4$^-$ (Fig. 4*E*). These cells may have been infected in the first few days of the infection and facilitated spread to the white matter (22). In summary, these results show that the number of microglia that survived infection with MHV differed when the brain and spinal cord were compared, but OLs predominated in general.

tdTomato$^+$ Cells Are Localized to Areas of Demyelination. Demyelination in MHV-infected mice occurs during the process of virus clearance (23–25), but it is not known whether cells that survive the acute infection are also localized to sites of myelin destruction. To determine the relationship between previously infected surviving cells and demyelination, we identified areas of myelin destruction using Black Gold Myelin staining, detected microglia/macrophage by immunohistochemistry, and correlated these myeloid cells with tdTomato$^+$ cells. Consistent with previous reports, areas of demyelination were present throughout the spinal cord, especially in the ventral part of the cervical and thoracic regions (20) (*SI Appendix*, Figs. S4 and S5*A*), but not the lumbar region (*SI Appendix*, Fig. S5*A*). Most tdTomato$^+$ cells at 30 d p.i. were located in areas of demyelination in association with activated microglia/macrophages (Fig. 5*B* and *SI Appendix*, Fig. S4). Activated microglia/macrophages had hyper-ramified, de-ramified, or amoeboid morphology. We quantified regional differences in microglia/macrophages using a previously described method (26) in which the numbers of branches and their length on individual microglia/macrophages were quantified as a measure of activation (an example is shown in *SI Appendix*, Fig. S5*B*). Numbers of branches and their lengths were shown to correlate with microglia/macrophage activation in several studies (26, 27).Greater numbers and lengths of branches were detected on microglia/macrophages in WMLs in the cervical and thoracic regions compared to cells in normal appearing white matter (NAWM) in the spinal cord (Fig. 5 *B* and *C* and *SI Appendix*, Fig. S5*B*). Notably, surviving cells were also detected in the rostral pons but were associated with only mild demyelination and less evidence of myeloid and CD8 T cell accumulation and activation as assessed morphologically (Fig. 5 *B* and *C* and *SI Appendix*, Fig. S6*B*). By 60 d p.i., tdTomato$^+$ cells were still present and associated with microglia/macrophages (Fig. 6 *A* and *B*), but demyelination had largely resolved (*SI Appendix*, Fig. S5*C*). Furthermore, microglia located near infected cells no longer had morphological changes suggestive of activation (Fig. 6 *A*–*C*). Together, these results show that microglia/macrophages and demyelination were spatially associated with previously infected cells and that the extent of demyelination was CNS region-dependent.

tdTomato$^+$ Surviving Cells Are Found in Areas of Microglia/Macrophage and CD8 T Cell Accumulation and Exhibit CNS Region-Dependent Differences in the Extent of OL Branch Formation. Demyelination in MHV-infected mice occurs after virus-specific T cells or, less commonly, virus-specific antibodies enter the CNS (23–25, 28). We next examined the rostral pons and spinal cord for the presence of infiltrating T cells at 30 dpi and detected CD8 T cells in areas of demyelination in the cervical and thoracic spinal cord, adjacent to tdTomato+ cells and microglia/macrophages (Fig. 5*B* and *SI Appendix*, Fig. S6). The infiltrating CD8 T cells were likely virus-specific because ∼80% of CD8 T cells infiltrating the infected brains and spinal cords of C57BL/6 mice recognize peptides encompassing two H-2^b–restricted peptides (D^b/S510 and K^b/S598) encoded by the MHV S protein (29, 30). Infected cells in the rostral pons were also associated with CD8 T cells although fewer CD8 T cells were present than in WMLs in the spinal cord. Together, these results indicate that, even though numbers of tdTomato$^+$ cells were similar in the rostral pons and cervical spinal cord, the number of associated activated myeloid and CD8 T cells was greater in the latter, concomitant with increased myelin destruction.

Remyelination is nearly complete by day 60 p.i. (8). In areas where demyelination was never extensive at 30 dpi, such as the rostral pons (*SI Appendix*, Fig. S6*A*), previously infected OLs exhibited extensive branch formation, suggesting that they were phenotypically normally myelinating oligodendrocytes (Fig. 6*A*). However, in areas in the spinal cord that exhibited substantial myelin destruction at day 30 p.i., we still detected colocalized CD8 T cells, microglia/macrophages, and surviving cells (Fig. 6 *B*, *D*–*F*, *SI Appendix*, Fig. S6, and Movie S1). Myeloid cells in these regions,

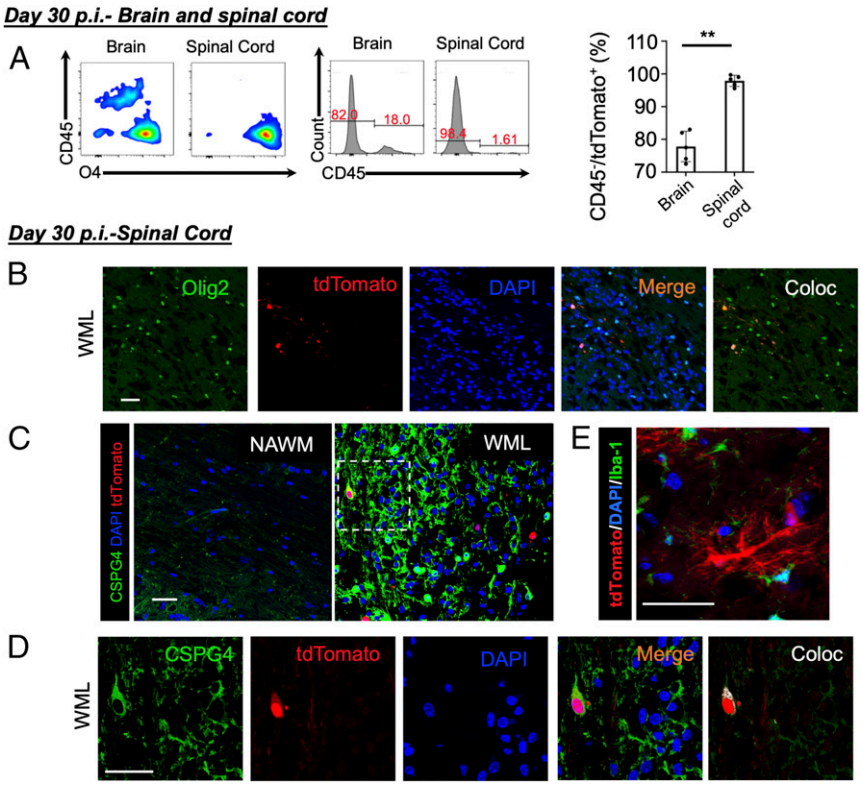

Fig. 4. Oligodendrocytes are the predominant surviving cells in the spinal cord. (*A*) Percentage of O4$^+$ oligodendrocytes in the brain and spinal cord at day 30 p.i. ($n = 5$ mice). TdTomato-positive cells were identified as shown in Fig. 2*A*. $^{**}P \leq 0.01$. (*B–D*) Sections of spinal cord were stained with oligodendrocyte lineage-specific antibodies (Olig2: OLs and OPCs; CSPG4: OPCs only). Most tdTomato$^+$ cells were OLs (*B*). (*C*) OPCs accumulated adjacent to demyelinating lesions in the spinal cord. tdTomato$^+$ OPCs were found in the WML. Boxed area in *C* is shown in *D*. $n = 5$ mice. Representative images are shown. (*E*) Surviving cells localized in the gray matter that had a neuron-like morphology. (*B–E*) Nuclei are stained with DAPI (blue). (Scale bars: 50 μm.)

as assessed by morphology, appeared less activated than at 30 dpi (compare Figs. 5*B* and 6*B*) and were morphologically similar in the rostral pons and spinal cord (Fig. 6*C*). A minority of surviving OLs in areas of previous demyelination showed evidence of branch formation, although less than that observed in the rostral pons (Fig. 6 *B* and *D*), consistent with OLs with some degree of remyelinating ability. However, many of the tdTomato$^+$ cells in the spinal cord, presumably localized to sites of WMLs that had resolved, had no evidence of process formation and were closely juxtaposed to CD8 T cells and microglia/macrophages (Fig. 6 *E* and *F* and Movie S1) Some of the surviving cells in WMLs were in the process of being phagocytosed by microglia/macrophages (boxed cell in Fig. 6*E* is shown at higher magnification in Fig. 6*F* and Movie S1).

MHC Class I Expression Is Elevated on OLs That Survive MHV Infection. Since CD8 T cells recognize antigens after presentation by MHC class I (MHC-I) molecules, we next examined O4$^+$ cells in the infected CNS for MHC-I expression by flow cytometry (Fig. 7 *A* and *B*). At day 15 p.i., O4$^+$ cells that had been previously infected as well as tdTomato$^-$ cells from infected mice up-regulated MHC-I expression, although expression was higher in tdTomato$^+$ cells (Fig. 7 *A* and *B*). MHC-I expression diminished on tdTomato$^-$ cells by day 30 p.i. and was back to baseline by day 40 p.i., while tdTomato$^+$ cells still expressed slightly elevated MHC-I levels even at day 90 p.i. (Fig. 7 *A* and *B*). Of note, while MHC class II (MHC-II) antigen was detectable on microglia/macrophages, we detected only a slight up-regulation of MHC-II antigen on oligodendrocytes at day 30 p.i. (*SI Appendix*, Fig. S7*A*).

Prior MHV Infection Induces Chronic Changes in Inflammatory Molecule Expression in Both tdTomato$^+$ and tdTomato$^-$ OLs. The expression of MHC-I by OLs in the CNS of surviving mice suggested that these cells were in a state of immune activation. To further investigate this possibility, we isolated tdTomato$^+$ and tdTomato$^-$ OLs from the brains and spinal cords of infected mice at 30 dpi and compared their transcriptomes to those of OLs isolated from mock-infected CNS samples by next-generation sequencing (gating strategy shown in *SI Appendix*, Fig. S7*B*). We identified 158 and 115 genes that showed a significant difference ($P < 0.05$) when tdTomato$^+$ and tdTomato$^-$ cells were compared to cells from mock-infected mice, respectively, with 61 messenger RNAs common to both tdTomato$^-$ and tdTomato$^+$ cells (Fig. 8 *A* and *B*). Many of these genes were involved in antigen presentation and response to IFN-γ (Fig. 8*C* and *SI Appendix*, Fig. S8 *A* and *B*). Consistent with up-regulation of MHC-I, several genes in the MHC-I antigen presentation pathway, including TAP1/2 and the heavy and light chains of MHC-I, were up-regulated Fig. 8*D*. Up-regulation of genes associated with response to IFN-γ may be a consequence of CD8 T cell activation by OLs expressing MHC class I. Additionally, genes involved in remyelination, such as *pdgfra*, *olig2*, *myrf*, and *mbp* were up-regulated when OLs from previously infected and mock-infected mice were compared (Fig. 8*C*). Several genes, such as *disp3*, *wnt7a*, *wnt7b*, and *gpr37L1*, are involved in inhibition of precursor cell differentiation and were down-regulated in OLs from infected mice ("negative regulation of neurogenesis" pathway, Fig. 8*C*).

Furthermore, genes associated with antigen presentation were up-regulated to a greater extent in tdTomato$^+$ compared to tdTomato$^-$ OLs (Fig. 8*E*, $P < 0.05$), consistent with Fig. 7 *A* and

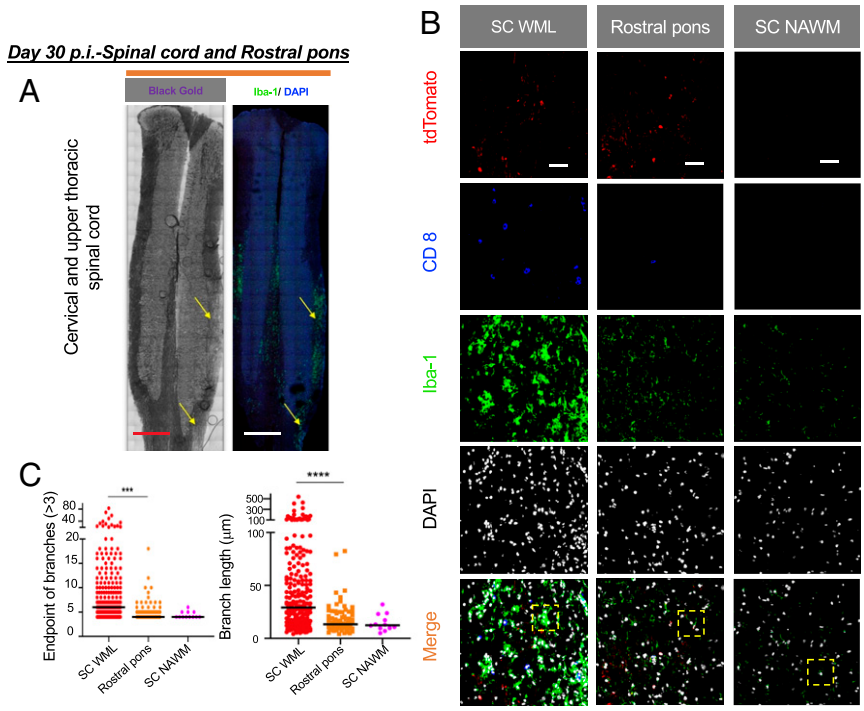

Fig. 5. All regions of demyelination in the spinal cord contain surviving OLs and show site-specific immune responses at day 30 p.i. (*A*) Sagittal sections of cervical and upper thoracic spinal cords from mice infected with $rMHV_{Cre}$ (750 PFUs) were prepared and stained with myelin gold (*Left*) or with anti–Iba-1 antibody (*Right*). Demyelinating lesions are indicated (yellow arrow). Extensive infiltration of myeloid cells is shown. (Scale bar: 1,000 μm.) (*B*) Sections of rostral pons, WMLs, and NAWM were immunolabeled for CD8 (blue) and Iba-1 (green) expression. More CD8 T cells and activated myeloid cells were detected in the WML than in the rostral pons even though numbers of surviving cells were similar. (*C*) Microglia/macrophages in *B* (Iba-1–stained) were converted to binary and skeleton images (The boxed areas in Fig. 5*B* are shown in *SI Appendix*, Fig. S5*B*, as an example of how we quantified branch length and endpoints.) Summary of microglia/macrophage endpoints/cell (*Left*) and process length/cell data (*Right*) in different regions that were measured as described in *Materials and Methods*. A cutoff value of three endpoint branches was used to minimize background effects. Microglia/macrophages in the spinal cord (SC) WML had increased numbers (*C*, *Left*) and increased length (*C*, *Right*) of branches, suggestive of increased activation. ***$P < 0.001$, ****$P < 0.0001$; one-way ANOVA; $n = 3$ mice and three sections/mouse.

B. Expression of genes in other pathways, including some involved in the cellular response to IFN-β and cytokine production, were also different when tdTomato$^+$ and tdTomato$^-$ cells were compared, although the direction of change was not uniform within each group (*SI Appendix*, Fig. S8*C*). Increased expression of genes associated with antigen presentation in tdTomato$^+$ compared to tdTomato$^-$ cells could reflect continued presence of residual viral antigen in tdTomato$^+$ cells. Together, these data indicate that widespread changes in inflammatory gene expression in OLs persist for at least 30 d after initiation of a CNS viral infection, contributing to a chronic inflammatory milieu, and that OLs that had been previously infected as well as cells that had never been infected contribute to this milieu.

Discussion

OLs are the most important target for infection in human diseases such as progressive multifocal leukoencephalopathy and HHV-6 encephalitis and are also in mice infected with Semliki forest virus or murine retroviruses (31–34). However, it is not known whether some or all of these cells actually survive the acute infection and whether the surviving cells contribute to demyelination or to a state of chronic inflammation. Furthermore, it is not known whether these cells eventually regain functionality and are able to effect remyelination. Here, we use a lineage tracing model to show that a fraction of previously infected OLs survive a neurotropic coronavirus infection and in some cases have the phenotype of normal myelin-producing cells. OLs in the acutely infected CNS during the resolution phase showed increased expression of genes involved in inflammation. This was true both for OLs that were previously infected and for OLs that were never infected. Strikingly, MHC-I expression was elevated on most OLs from infected brains and spinal cords, when compared to those from mock-infected mice. MHC-I expression remained elevated for at least 90 d, with levels higher on previously infected OLs (Fig. 7). tdTomato$^+$ OLs may have expressed low levels of virus antigen, explaining their prolonged MHC-I expression, compared to OLs that were never infected. In nearly all reports, viral antigen cannot be detected after 1 to 2 wk after MHV infection. However, if naive T cells are transferred into previously infected mice at times as late as 33 dpi, an outgrowth of MHV-specific CD8 T cells can be identified in the brain and spinal cord, consistent with priming in the lymph nodes and de novo production of MHV-specific T cells (13). Other studies have demonstrated MHV RNA persistence for at least 100 dpi (11, 12). Although not identified in our study, the presence of residual viral RNA and antigen, both below the level of detection, may explain why MHC-I levels were prolonged on the previously infected OLs. Prolonged MHC-I expression on OLs that were never infected may reflect exposure to proinflammatory cytokines, especially IFN-γ (35–37)

Until recently, OLs were not considered to be part of the inflammatory process in diseases such as MS and its rodent model, EAE. However, OLs and OPCs have been shown to express MHC-I as well as other genes involved in antigen presentation and inflammation in the context of EAE and of cuprizone-induced demyelination (6, 7). Our results extend these previous reports to neurotropic viral infections and suggest a plausible model for how virus infection could contribute to disease in patients with MS. While viral infections have been implicated in

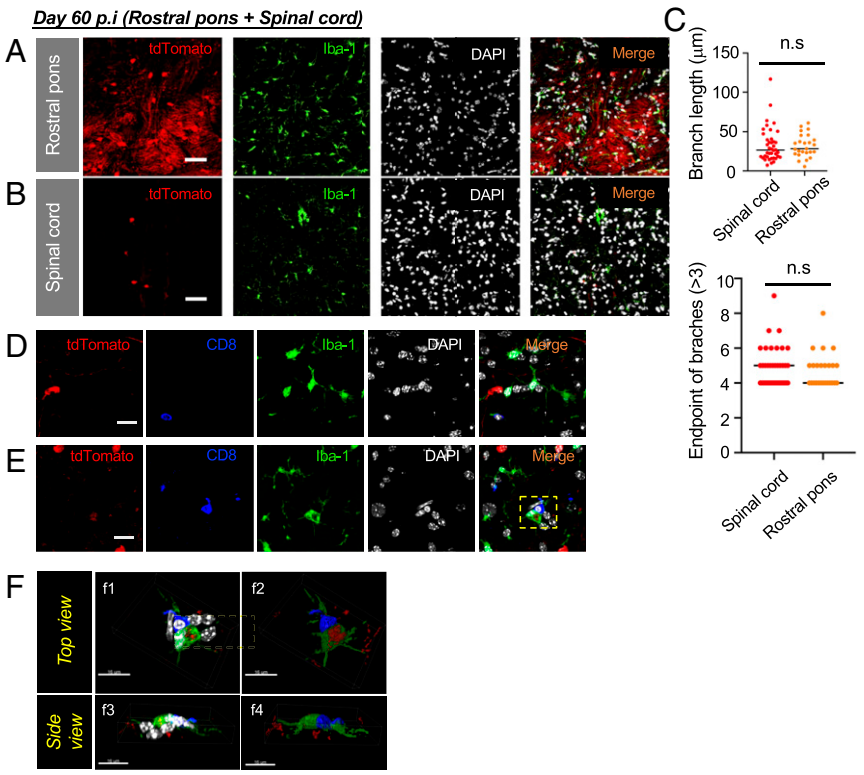

Fig. 6. Surviving OLs exhibit site-specific morphology and variable degrees of inflammation at 60 dpi. Sections were prepared from the rostral pons (*A*) and spinal cord (*B*, *D*, and *F*) and immunolabeled with Iba-1. Surviving cells in the rostral pons showed evidence of process extension consistent with remyelinating function and were associated with microglia/macrophages that had nearly normal morphology (*A*). tdTomato$^+$ cells in the spinal cord were associated with activated myeloid cells and CD8 T cells (blue) (*B*, *D*, and *E*) and either remained rounded (*E*) or showed minimal process extension (*D*) compared to cells in the rostral pons. (*C*) Microglia/macrophages in *A* and *B* (Iba-1–stained) were converted to binary and skeleton images. Summary of microglia/macrophages process length/cell (*Top*) and endpoints/cell (*Bottom*) in different regions that were measured as described in *Materials and Methods*, n.s., not significant. (*F*) A tdTomato$^+$ cell undergoing engulfment by a myeloid cell (from boxed area of *E*) is shown. Iso-surface rendition (*f2*, *f4*) obtained from the stacks (*f1*, *f3*) using Imaris is shown. (Scale bar: *A* and *B*, 50 μm; *D* and *E*, 20 μm; *F*, 16 μm.)

the initiation and relapse of MS, their exact role remains poorly understood. Very low levels of viral antigen in oligodendrocytes after a subclinical infection could contribute to a prolonged inflammatory response and ongoing demyelination. In addition, infection of OPCs, as observed in MHV-infected mice, may contribute to delayed remyelination. Whether newly arising OLs or, alternatively, mature OLs contribute to remyelination remains an area of investigation (38). Newly recruited and preexisting mature OLs are found in areas of remyelination in rodents, but only the former appear to be capable of remyelination (39, 40). In contrast, human studies suggest that remyelination is accomplished largely by preexisting mature OLs (41). OPCs may

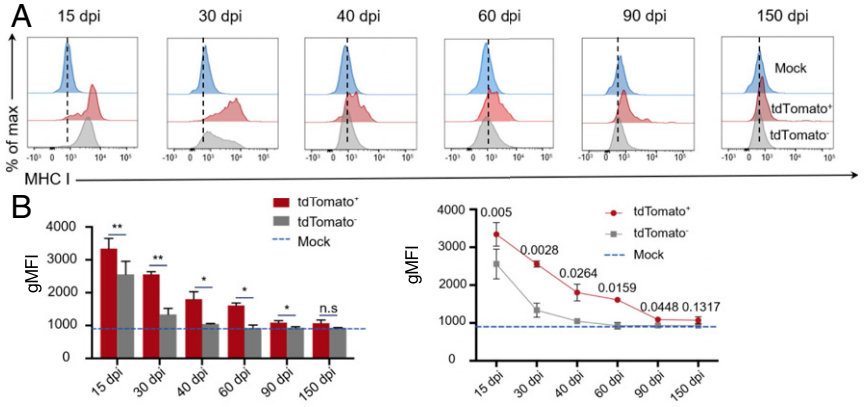

Fig. 7. Long-term MHC class I up-regulation on tdTomato$^+$ OLs. (*A* and *B*) OLs from uninfected and infected mice at day 30 p.i. were stained for MHC-I expression and analyzed by flow cytometry (mock-blue, tdTomato$^+$-red, tdTomato$^-$-gray) . Both tdTomato$^+$ and tdTomato$^-$ OLs up-regulated MHC-I, but up-regulation was more prolonged on tdTomato+ cells. Dashed line indicates MHC-I in mock-infected mice (normalized). Geometric mean fluorescence intensity (gMFI) data are summarized in *B*. Data are means ± SD of five mice/time point. $*P < 0.05$, $**P < 0.01$; Student's *t* test for indicated pairwise comparison, coupled with one-way ANOVA for multigroup comparisons.

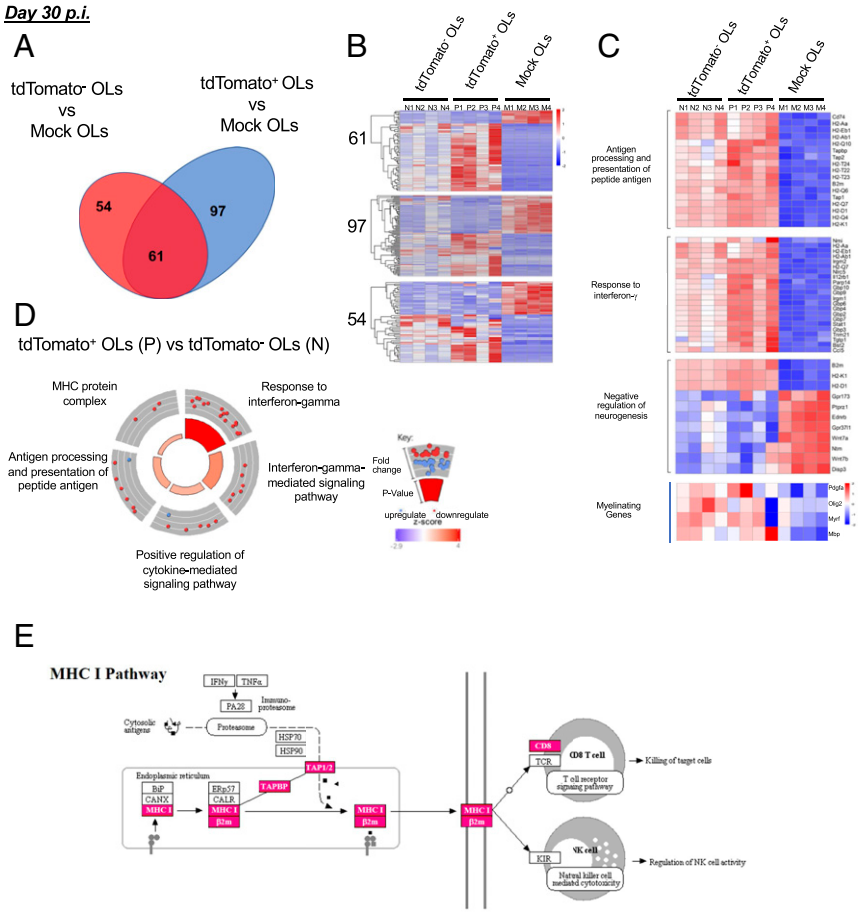

Fig. 8. Next generation RNA-Seq analyses of gene expression profile in $rMHV_{Cre}$-infected and noninfected OLs at 30 d p.i. Gene expression analyses were performed using four independent biological replicates (tdTomato$^+$ OLs [P], tdTomato$^-$ OLs [N] from infected mice and OLs from mock-infected mice [M]). (*A* and *B*) Venn diagram (*A*) and heat map (*B*) summarizing the number and overlap of genes regulated in P versus M (blue) or N versus M (red). (*C* and *D*) Heat map (*C*) and circle plots (*D*) comparing targeted pathways, including antigen presentation, identified by pathway analysis. There is increased expression of antigen presentation and response to IFN-γ pathways in P compared to N. In *D*, the outer circle scatter plots represent differential gene expression within each term, with red points representing up-regulated genes and blue points representing down-regulated genes. The inner circle is colored based on Z score, which is a measure for predicting a bias in gene regulation, with blue predicting a decrease in the pathway and red predicting an increase. Additionally, the inner circle is sized based on *P* value, with the larger size correlating to a more significant *P* value. (*E*) MHC I antigen expression and related genes as depicted in the KEGG: Kyota Encyclopedia of Genes and Genomes database are shown. Red boxes denote up-regulated genes, when groups N and P were compared to M.

proliferate and become OLs, or mature without proliferation, contributing to remyelination. We detected previously infected OPCs in the subventricular zone at days 30 and 60 p.i. and in the spinal cord in areas of demyelination at day 30. The latter observation suggests that prior infection did not impair the ability of OPCs to migrate to sites of demyelination, but future work will be required to determine whether these cells are fully functional.

One striking feature is that while tdTomato$^+$ OLs display similar morphological changes throughout the spinal cord at 30 dpi, their morphology and likely functionality display CNS region-specific differences by 60 dpi (Fig. 6 *A* and *B*). These differences were correlated with differences in myeloid cell infiltration and activation (Fig. 5 *B* and *C*). Thus, tdTomato$^+$ OLs in the rostral pons, most likely in the area of the corticospinal tract, extended long processes consistent with remyelinating function, while those in the spinal cord, even in the area of the corticospinal tract, remained rounded up and were associated with demyelinating lesions. While these regional differences in the immune response to MHV and in oligodendrocyte morphology of surviving cells are unexpected, there is precedent for regional differences in the brain and spinal cord for immune responses and gene expression. For example, while antibodies are critical for clearance of Sindbis virus from the brain, T cells expressing IFN-γ were able to clear virus from neurons in the brainstem and cortex but not cortex (42). Most research has focused on regional differences in gene expression in development and homeostasis, but our results suggest that similar differences impact immune function.

In summary, OLs and OPCs that were previously infected with a neurotropic virus often survive the acute infection and remain immunologically active. Their presence in areas of demyelination may be a nidus for an ongoing inflammatory response with continued myelin destruction (pathogenic), but may also contribute to remyelination (protective). Thus, oligodendrocytes not only are the target of the immune response, but also actively contribute to its development. Further work will be directed at discovering the factors that determine whether OLs will be pathogenic or protective and whether these factors can be manipulated to enhance myelin regeneration in demyelinating lesions.

Materials and Methods

Mice. Specific-pathogen-free C57Bl/6 mice were purchased from Charles River Laboratories. B6.Cg-*Gt(ROSA)26Sor*$^{tm14(CAG-tdTomato)Hze}$/J (tdTomato) mice were purchased from Jackson Laboratories. Mice were maintained in specific pathogen-free facilities at The University of Iowa. Male mice were

used in these experiments because although similar results were obtained with female mice, results were less consistent. Five- to seven-week-old mice were intracranially inoculated with 750 PFU rMHV, $rMHV_{Cre}$ or $rMHV_{Venus}$ after isoflurane anesthesia. After virus inoculation, mice were observed and weighed daily. All animal studies were approved by the University of Iowa Animal Care and Use Committee and meet stipulations of the Guide for the Care and Use of Laboratory Animals (43).

Generation of Recombinant MHV_{Cre}. Cre recombinase was cloned into pBAC (plasmid bacterial artificial chromosome)-MHV as previously described (44). Briefly, a PCR product containing Cre-FRT-Kan^r-FRT and 5′ and 3′ homology to the regions just outside ORF4 was created using two-step PCR. A plasmid containing Cre sequence was a gift from Benjamin tenOever, Icahn Mt. Sinai School of Medicine. This cassette was transformed into *Escherichia coli* containing pBAC-rJ2.2. rJ2.2 is a neuroattenuated version of the JHMV strain of MHV (45). Bacteria with successfully recombined pBAC-MHV were identified by kanamycin resistance. Correct clones were amplified and treated with *Flp* recombinase to excise the kanamycin resistance cassette surrounded by Flp recombination targets. pBAC-derived $rMHV_{Cre}$ was obtained after transfection as previously described (44). $rMHV_{Cre}$ virus was grown on 17Cl-1 cells, and virus titers were determined on HeLa cells expressing the MHV receptor (17). $rMHV_{Venus}$ was generated using the same strategy as used for $rMHV_{Cre}$, Venus was PCR-amplified from pSLIK-Venus (plasmid #25734, purchased from Addgene).

Additional figures (*SI Appendix*, Figs. S1–S8) supporting the main text are provided in *SI Appendix*. A full overview of the methods, materials, and data referred to in this study is available in *SI Appendix*.

Data Availability. Next-generation RNA sequence data supporting the findings in this study have been deposited in the Gene Expression Omnibus database (https://www.ncbi.nlm.nih.gov/geo/) under accession number GSE148650.

ACKNOWLEDGMENTS. We thank Drs. Anthony Fehr and Rudragouda Channappanavar for help with the MHV reverse genetics system; Dr. Jian Zheng for help with the flow cytometry; and Alan Sariol for critical review of the manuscript. We acknowledge use of the University of Iowa Central Microscopy Research Facility and Flow Cytometry Facility, a core resource supported by the Vice President for Research & Economic Development, the Holden Comprehensive Cancer Center, and the Carver College of Medicine. This work was supported in part by grants from the NIH (RO1 NS36592) and National Multiple Sclerosis Society (RG 5340-A-7).

1. C. A. Dendrou, L. Fugger, M. A. Friese, Immunopathology of multiple sclerosis. *Nat. Rev. Immunol.* **15**, 545–558 (2015).
2. R. Dobson, G. Giovannoni, Multiple sclerosis: A review. *Eur. J. Neurol.* **26**, 27–40 (2019).
3. S. Kuhn, L. Gritti, D. Crooks, Y. Dombrowski, Oligodendrocytes in development, myelin generation and beyond. *Cells* **8**, 1424 (2019).
4. S. Marques *et al.*, Oligodendrocyte heterogeneity in the mouse juvenile and adult central nervous system. *Science* **352**, 1326–1329 (2016).
5. A. B. Rosenberg *et al.*, Single-cell profiling of the developing mouse brain and spinal cord with split-pool barcoding. *Science* **360**, 176–182 (2018).
6. L. Kirby *et al.*, Oligodendrocyte precursor cells present antigen and are cytotoxic targets in inflammatory demyelination. *Nat. Commun.* **10**, 3887 (2019).
7. A. M. Falcão *et al.*, Disease-specific oligodendrocyte lineage cells arise in multiple sclerosis. *Nat. Med.* **24**, 1837–1844 (2018).
8. C. C. Bergmann, T. E. Lane, S. A. Stohlman, Coronavirus infection of the central nervous system: Host-virus stand-off. *Nat. Rev. Microbiol.* **4**, 121–132 (2006).
9. C. Huang *et al.*, Clinical features of patients infected with 2019 novel coronavirus in Wuhan, China. *Lancet* **395**, 497–506 (2020).
10. Q. Li *et al.*, Early transmission dynamics in Wuhan, China, of novel coronavirus-infected pneumonia. *N. Engl. J. Med.* **382**, 1199–1207 (2020).
11. C. L. Rowe, S. C. Baker, M. J. Nathan, J. O. Fleming, Evolution of mouse hepatitis virus: Detection and characterization of spike deletion variants during persistent infection. *J. Virol.* **71**, 2959–2969 (1997).
12. C. Adami *et al.*, Evolution of mouse hepatitis virus (MHV) during chronic infection: Quasispecies nature of the persisting MHV RNA. *Virology* **209**, 337–346 (1995).
13. J. Zhao, J. Zhao, S. Perlman, De novo recruitment of antigen-experienced and naive T cells contributes to the long-term maintenance of antiviral T cell populations in the persistently infected central nervous system. *J. Immunol.* **183**, 5163–5170 (2009).
14. N. S. Heaton *et al.*, Long-term survival of influenza virus infected club cells drives immunopathology. *J. Exp. Med.* **211**, 1707–1714 (2014).
15. E. A. Gomme, C. Wirblich, S. Addya, G. F. Rall, M. J. Schnell, Immune clearance of attenuated rabies virus results in neuronal survival with altered gene expression. *PLoS Pathog.* **8**, e1002971 (2012).
16. E. Ontiveros, L. Kuo, P. S. Masters, S. Perlman, Inactivation of expression of gene 4 of mouse hepatitis virus strain JHM does not affect virulence in the murine CNS. *Virology* **289**, 230–238 (2001).
17. L. Pewe *et al.*, A severe acute respiratory syndrome-associated coronavirus-specific protein enhances virulence of an attenuated murine coronavirus. *J. Virol.* **79**, 11335–11342 (2005).
18. E. M. Barnett, M. D. Cassell, S. Perlman, Two neurotropic viruses, herpes simplex virus type 1 and mouse hepatitis virus, spread along different neural pathways from the main olfactory bulb. *Neuroscience* **57**, 1007–1025 (1993).
19. E. Lavi, D. H. Gilden, M. K. Highkin, S. R. Weiss, Persistence of mouse hepatitis virus A59 RNA in a slow virus demyelinating infection in mice as detected by in situ hybridization. *J. Virol.* **51**, 563–566 (1984).
20. S. Perlman, G. Jacobsen, A. L. Olson, A. Afifi, Identification of the spinal cord as a major site of persistence during chronic infection with a murine coronavirus. *Virology* **175**, 418–426 (1990).
21. J. J. Houtman, J. O. Fleming, Pathogenesis of mouse hepatitis virus-induced demyelination. *J. Neurovirol.* **2**, 361–376 (1996).
22. N. Sun, S. Perlman, Spread of a neurotropic coronavirus to spinal cord white matter via neurons and astrocytes. *J. Virol.* **69**, 633–641 (1995).
23. F. I. Wang, S. A. Stohlman, J. O. Fleming, Demyelination induced by murine hepatitis virus JHM strain (MHV-4) is immunologically mediated. *J. Neuroimmunol.* **30**, 31–41 (1990).
24. J. J. Houtman, J. O. Fleming, Dissociation of demyelination and viral clearance in congenitally immunodeficient mice infected with murine coronavirus JHM. *J. Neurovirol.* **2**, 101–110 (1996).
25. G. F. Wu, A. A. Dandekar, L. Pewe, S. Perlman, CD4 and CD8 T cells have redundant but not identical roles in virus-induced demyelination. *J. Immunol.* **165**, 2278–2286 (2000).
26. H. W. Morrison, J. A. Filosa, A quantitative spatiotemporal analysis of microglia morphology during ischemic stroke and reperfusion. *J. Neuroinflammation* **10**, 4 (2013).
27. K. Young, H. Morrison, Quantifying microglia morphology from photomicrographs of immunohistochemistry prepared tissue using imageJ. *J. Vis. Exp.*, 57648 (2018).
28. T. S. Kim, S. Perlman, Virus-specific antibody, in the absence of T cells, mediates demyelination in mice infected with a neurotropic coronavirus. *Am. J. Pathol.* **166**, 801–809 (2005).
29. R. F. Castro, S. Perlman, CD8+ T-cell epitopes within the surface glycoprotein of a neurotropic coronavirus and correlation with pathogenicity. *J. Virol.* **69**, 8127–8131 (1995).
30. S. Xue, S. Perlman, Antigen specificity of CD4 T cell response in the central nervous system of mice infected with mouse hepatitis virus. *Virology* **238**, 68–78 (1997).
31. J. K. Fazakerley, Pathogenesis of Semliki forest virus encephalitis. *J. Neurovirol.* **8** (suppl. 2), 66–74 (2002).
32. A. C. Clase *et al.*, Oligodendrocytes are a major target of the toxicity of spongiogenic murine retroviruses. *Am. J. Pathol.* **169**, 1026–1038 (2006).
33. A. J. Aksamit Jr., Progressive multifocal leukoencephalopathy: A review of the pathology and pathogenesis. *Microsc. Res. Tech.* **32**, 302–311 (1995).
34. R. H. Swanborg, J. A. Whittum-Hudson, A. P. Hudson, Human herpesvirus 6 and Chlamydia pneumoniae as etiologic agents in multiple sclerosis: A critical review. *Microbes Infect.* **4**, 1327–1333 (2002).
35. L. Pewe, S. Perlman, Cutting edge: CD8 T cell-mediated demyelination is IFN-gamma dependent in mice infected with a neurotropic coronavirus. *J. Immunol.* **168**, 1547–1551 (2002).
36. S. P. Templeton, S. Perlman, Role of IFN-gamma responsiveness in CD8 T-cell-mediated viral clearance and demyelination in coronavirus-infected mice. *J. Neuroimmunol.* **194**, 18–26 (2008).
37. L. Hamo, S. A. Stohlman, M. Otto-Duessel, C. C. Bergmann, Distinct regulation of MHC molecule expression on astrocytes and microglia during viral encephalomyelitis. *Glia* **55**, 1169–1177 (2007).
38. J. R. Plemel, W.-Q. Liu, V. W. Yong, Remyelination therapies: A new direction and challenge in multiple sclerosis. *Nat. Rev. Drug Discov.* **16**, 617–634 (2017).
39. E. G. Hughes, S. H. Kang, M. Fukaya, D. E. Bergles, Oligodendrocyte progenitors balance growth with self-repulsion to achieve homeostasis in the adult brain. *Nat. Neurosci.* **16**, 668–676 (2013).
40. H. S. Keirstead, W. F. Blakemore, Identification of post-mitotic oligodendrocytes incapable of remyelination within the demyelinated adult spinal cord. *J. Neuropathol. Exp. Neurol.* **56**, 1191–1201 (1997).
41. M. S. Y. Yeung *et al.*, Dynamics of oligodendrocyte generation in multiple sclerosis. *Nature* **566**, 538–542 (2019).
42. G. K. Binder, D. E. Griffin, Interferon-gamma-mediated site-specific clearance of alphavirus from CNS neurons. *Science* **293**, 303–306 (2001).
43. National Research Council, *Guide for the Care and Use of Laboratory Animals*, (National Academies Press, Washington, DC, ed. 8, 2011).
44. A. R. Fehr *et al.*, The nsp3 macrodomain promotes virulence in mice with coronavirus-induced encephalitis. *J. Virol.* **89**, 1523–1536 (2015).
45. J. O. Fleming, M. D. Trousdale, F. A. el-Zaatari, S. A. Stohlman, L. P. Weiner, Pathogenicity of antigenic variants of murine coronavirus JHM selected with monoclonal antibodies. *J. Virol.* **58**, 869–875 (1986).